Journal of Hydrology (2008) 352, 211–224

available at www.sciencedirect.com

ScienceDirect

journal homepage: www.elsevier.com/locate/jhydrol

Tide-induced seawater–groundwater circulation in shallow beach aquifers

Hailong Li [a,b], Michel C. Boufadel [a,*], James W. Weaver [c]

[a] *Department of Civil and Environmental Engineering, Temple University, 1947 North 12th Street, Philadelphia, PA 19122, USA*
[b] *School of Environmental Studies and (MOE) Biogeology and Environmental Geology Laboratory, China University of Geosciences, Wuhan 430074, PR China*
[c] *National Exposure Research Laboratory, US EPA, Athens, GA 30605, USA*

Received 7 July 2007; received in revised form 7 January 2008; accepted 18 January 2008

KEYWORDS
Beach slope;
Dimensionless model;
Seepage face;
Intertidal zone;
Seawater–groundwater circulation;
Solute transport

Summary In this paper, we investigated the tide-induced seawater–groundwater circulation in shallow beach aquifers using the finite element model MARUN. The numerical solutions were generalized using a dimensionless formulation. From a dimensionless tidal period and a dimensionless beach slope of 10%, we obtained results that apply to a wide range of beach permeabilities from 10^{-4} m/s to 10^{-3} m/s, beach slopes from 3.16% to 31.6%, tidal amplitude (0.3 m-2 m) and period (diurnal or semidiurnal). The numerical simulations demonstrated the following: The maximum Darcy velocity always occurs at the intersection of the watertable and the beach surface. The offshore beach groundwater is almost stagnant compared with the onshore groundwater flow, which may explain the previous observations that the major portion of the seaward groundwater seepage usually occurs in the shallow part of the submerged beach. The outflow from the seepage face accounts for 41–97% (average 55%) of the outflow from the intertidal zone. The amount of seawater infiltrating into the intertidal zone in a tidal cycle increases with the beach permeability and decreases when the inland recharge increases, and ranges from 35.5 $m^3\ yr^{-1}\ m^{-1}$ to 505.8 $m^3\ yr^{-1}\ m^{-1}$ for all the cases considered. Smaller beach slopes, smaller inland freshwater recharges, and/or greater beach permeability lead to larger saltwater plumes in the intertidal zone of the beach. The results are in line with the existing results of field observations and numerical simulations by previous researchers.
© 2008 Elsevier B.V. All rights reserved.

* Corresponding author. Tel.: +1 215 204 7871; fax: +1 215 204 4696.
E-mail addresses: hailong@temple.edu (H. Li), boufadel@temple.edu (M.C. Boufadel), Weaver.Jim@epamail.epa.gov (J.W. Weaver).

0022-1694/$ - see front matter © 2008 Elsevier B.V. All rights reserved.
doi:10.1016/j.jhydrol.2008.01.013

Introduction

Beaches and intertidal zones play important roles in coastal ecological systems and biodiversity because of the interactions of freshwater from inland and the seawater from the ocean as well as the combined actions of the tides and waves. Therefore, it is important to understand the dynamics of exchange of saltwater and freshwater along with water flows. Such an understanding is also needed if bioremediation is adopted following an oil spill on a beach (Venosa et al., 1996; Li et al., 2007). Numerous analytical (e.g., Nielsen, 1990; Li et al., 2000; Teo et al., 2003; Jeng et al., 2005; Cartwright et al., 2006; Li et al., 2007b; Li et al., 2007c), numerical (e.g., Turner, 1993; Li et al., 2005; Mao et al., 2006; Robinson et al., 2006; Werner and Lockington, 2006; Li et al., 2007a; Robinson et al., 2007), and experimental (e.g., Nielsen, 1990; Turner, 1993; Wrenn et al., 1997; Uchiyama et al., 2000; Cartwright et al., 2004; Robinson et al., 2006) studies have been conducted for the groundwater hydraulics and/or solute transport in coastal aquifer systems. Recently, the tidal effects on the submarine groundwater discharge in subterranean estuaries have been frequently investigated with field measurements and numerical simulations (e.g., Taniguchi, 2002; Li and Jiao, 2003; Prieto and Destouni, 2005; Robinson et al., 2006; Taniguchi et al., 2006; Robinson et al., 2007). Even in the absence of waves on beaches, rigorous quantification of beach hydraulics is challenging because of non-linearity resulting from both the dependence of water density on salt concentration (Frind, 1982) and water flow in the unsaturated zone. The presence of a seepage face introduces additional non-linearity due to the fact that the seepage face location cannot be known a priori (Neuman, 1973; Boufadel, 2000; Naba et al., 2002).

Various studies elucidated salinity distribution within the beach. Examples include the laboratory scale and numerical works of Ataie-Ashtiani et al. (1999b) and Boufadel (2000). The primary goal of this article is to evaluate exchange flows of the beach with both the sea and the landward aquifer. A secondary goal is to further elucidate the dynamics in tidally-influenced beaches.

The beach domain to be investigated is reported in Fig. 1a. The vertical extent of domain is L_z^*. The tide is assumed to be sinusoidal with a period T^*, and the tidal sea level is given by

$$h_{sea}^*(t^*) = h_m^* + A^* \cos\left(\frac{2\pi}{T^*} t^*\right), \quad (1)$$

where t^* is time and h_m^* is the mean sea level, and $A^* = L_z^*/5$ is the tidal amplitude (Fig. 1a). Starred quantities are dimensional and they will be converted in this manuscript to non-dimensional where then the stars are removed.

In contrast with the existing numerical studies with deep coastal aquifers (20-150 m) such as Prieto and Destouni (2005), Werner and Lockington (2006), and Robinson et al. (2006, 2007), here we only focused on relatively shallow beach aquifers shown in Fig. 1a. Shallow aquifers are commonplace in reality, e.g., the sandy beach aquifer on the southwestern shore of Delaware Bay (Wrenn et al., 1997), the aquifers of the Florida coast reported by Cable et al. (1997) and the glacial deposits along the North East coast of the USA (Valiela, 1990; Portnoy et al., 1998). In addition, studies have noted that the major portion of the seaward groundwater seepage usually occurs in the shallow part of the submerged beach and the magnitude of the seaward groundwater seepage decreases with seaward distance away from the coast (Bokuniewicz, 1980; Cable et al., 1997; Taniguchi, 2002; Slomp and Van Capellen, 2004; Taniguchi et al., 2006). Thus, even for deep aquifers, understanding the exchange occurring in the shallow part is of major importance.

The layout of the paper is as follows: First a dimensionless formulation is introduced to highlight the relative role of important mechanisms, and to generalize the results to beaches of various properties, such as the hydraulic conduc-

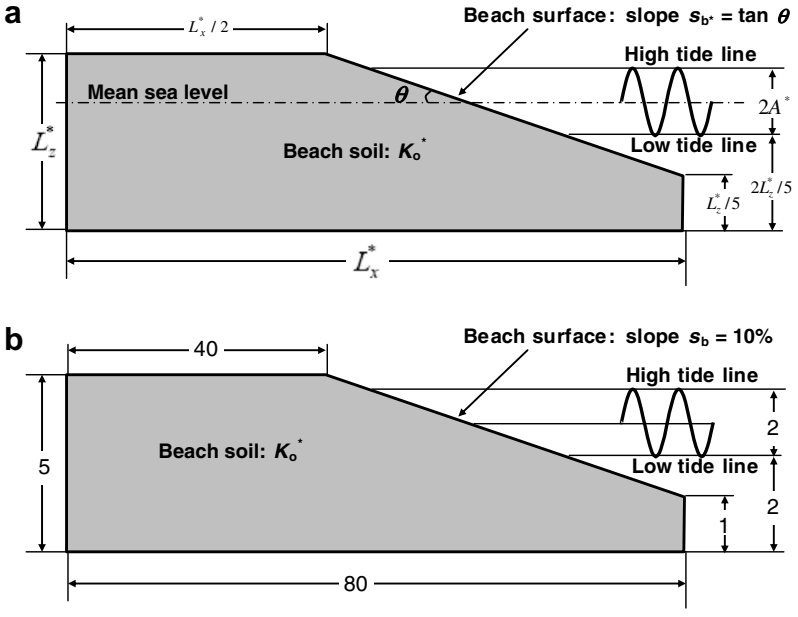

Figure 1 Beach cross-sectional domains for (a) real dimensional and (b) dimensionless model formulations.

tivity and the slopes on the sea side. Then the finite element code MARUN (Boufadel et al., 1999b) is used to obtain the numerical solutions of the dimensionless equations. Finally the results are presented.

Model description

Governing equations

Dimensional governing equations

Neglecting the elastic storage of the matrix, and using the formulation presented by Boufadel et al. (1999b) and Boufadel (2000), the water flow equation for two-dimensional density-dependent flow in homogeneous and isotropic media can be written as:

$$\phi\frac{\partial(\beta S)}{\partial t^*}=\frac{\partial}{\partial x^*}(\beta k_r K_0^*\frac{\partial\psi^*}{\partial x^*})+\frac{\partial}{\partial z^*}\left[\beta k_r K_0^*\left(\frac{\partial\psi^*}{\partial z^*}+\beta\right)\right], \tag{2}$$

where x^* [L], z^* [L] are the horizontal and vertical coordinates for the dimensional domain; ψ^* [L] is the pressure head, ϕ is the porosity, S is the degree of water saturation (fraction of pore volume occupied by water), K_0^* [LT^{-1}] is the saturated hydraulic conductivity of the beach, k_r is the relative permeability, β is the density ratio defined as

$$\beta=\frac{\rho^*}{\rho_0^*}=1+\varepsilon^* c^*\geqslant 1, \tag{3}$$

where ρ^* [ML^{-3}] is the density of the beach pore water, $\rho_0^*=998.2\ \mathrm{kg\ m^{-3}}$ is the fresh water density at 20 °C, ε^* is a constant equal to $6.46\times10^{-4}\ \mathrm{m^3\ kg^{-1}}$, c^* is the salt concentration [ML^{-3}] of the beach pore water.

The soil moisture ratio and the relative permeability are correlated by the van Genuchten (1980) model:

$$\text{For } \psi^*\geqslant 0: \quad S=1.0, \quad k_r=1. \tag{4a}$$

$$\text{For } \psi^*<0, \quad k_r=S_e^{0.5}[1-(1-S_e^{1/m})^m]^2, \tag{4b}$$

where S_e is the effective saturation ratio given by

$$S_e=\frac{S-S_r}{1-S_r}=\left[\frac{1}{1+(\alpha^*|\psi^*|)^n}\right]^m, \tag{4c}$$

where $m=1-\frac{1}{n}$, S_r is the residual saturation ratio, α^* [L^{-1}] represents the characteristic pore size of the beach soil, and higher α^* values imply a coarser material. The inverse of α^* provides an estimate of the static capillary fringe. The term n represents the uniformity of the pores and higher values of n imply a more uniform pore-size distribution (van Genuchten, 1980; Wise et al., 1994).

The solute transport equation is the well-known convection–dispersion equation rewritten by Boufadel et al. (1999a,c) as

$$\phi S\frac{\partial c^*}{\partial t^*}=\beta\nabla^*\cdot(\phi S D_f^*\nabla^* c^*)-\mathbf{q}^*\cdot\nabla^* c^*, \tag{5}$$

where D_f is the constant dispersion coefficient, and $\nabla^*=(\frac{\partial}{\partial x^*},\frac{\partial}{\partial z^*})$ is the gradient operator with respect to the dimensional spatial variables, $\mathbf{q}^*=(q_x^*,q_z^*)$ [LT^{-1}] is the Darcy flux vector defined as (Li et al., 2007a)

$$\mathbf{q}^*=(q_x^*,q_z^*)=-k_r K_0^*\left(\frac{\partial\psi^*}{\partial x^*},\frac{\partial\psi^*}{\partial z^*}+\beta\right). \tag{6}$$

Dimensionless formulation

Given a domain geometry, a tidal amplitude and period, and beach properties, solution of Eqs. (2) through (6) provides beach dynamics, and subsequently the exchange flow in and out of the beach domain. However, such an approach does not explain the relative role of various factors, and does not allow one to transpose the results to beaches of different properties or to beaches subjected to different tidal period or amplitude. For this reason, we will non-dimensionalize the equations following the methodology of Boufadel et al. (1999c,b) and Boufadel (2000).

Let:

$$x=\frac{x^*}{X_S^*},\quad z=\frac{z^*}{Z_S^*},\quad z=\frac{\psi^*}{Z_S^*},\quad t=\frac{t^*}{T_S^*},\quad \alpha=\alpha^* Z_S^*, \tag{7}$$

where X_S^* and Z_S^* are arbitrary horizontal and vertical scaling factors. For example, $X_S^*=5.0$ m and $Z_S^*=2.0$ m. The term T_S^* is a characteristic time scale that is defined as

$$T_S^*=\frac{Z_S^*}{K_0^*}. \tag{8}$$

Thus, x, z are the horizontal and vertical coordinates for the dimensionless domain, and t is dimensionless time.

Eq. (2) can thus be rewritten in a dimensionless form as

$$\phi\frac{\partial(\beta S)}{\partial t}=M\frac{\partial}{\partial x}\left(\beta k_r\frac{\partial\psi}{\partial x}\right)+\frac{\partial}{\partial z}\left[\beta k_r\left(\frac{\partial\psi}{\partial z}+\beta\right)\right]. \tag{9}$$

For isotropic domains, the parameter M is defined as (Boufadel, 2000)

$$M=\left(\frac{Z_S^*}{X_S^*}\right)^2=\left(\frac{s_{b*}}{s_b}\right)^2. \tag{10}$$

The effective water saturation ratio S_e defined by (2f) is unchanged:

$$S_e=\left[\frac{1}{1+(\alpha^*|\psi^*|)^n}\right]^m=\left[\frac{1}{1+(\alpha|\psi|)^n}\right]^m. \tag{11}$$

The dimensionless form of the solute transport equation is (Li et al., 2007a)

$$\phi S\frac{\partial c^*}{\partial t}=M\beta\frac{\partial}{\partial x}\left(\phi S D_f\frac{\partial c^*}{\partial x}\right)+\beta\frac{\partial}{\partial z}\left(\phi S D_f\frac{\partial c^*}{\partial z}\right)-\mathbf{q}\cdot\nabla c^*, \tag{12}$$

where D_f is the dimensionless dispersion coefficient defined as

$$D_f=\frac{D_f^*}{Z_S^* K_0^*}, \tag{13}$$

$\nabla=(\frac{\partial}{\partial x},\frac{\partial}{\partial z})$ is the gradient operator with respect to the dimensionless spatial variables, $\mathbf{q}=(q_x,q_z)$ is the dimensionless Darcy flux vector in the dimensionless domain:

$$\mathbf{q}=(q_x,q_z)=-k_r\left(M\frac{\partial\psi}{\partial x},\frac{\partial\psi}{\partial z}+\beta\right). \tag{14}$$

This implies that the original dimensional domain in Fig. 1a is transformed into the dimensionless domain in Fig. 1b with dimensionless height and length given by

$$L_z=\frac{L_z^*}{Z_S^*}\quad\text{and}\quad L_x=\frac{L_x^*}{X_S^*}. \tag{15}$$

The beach slope of the dimensionless domain (s_b) is related to that of the dimensional (real) domain (s_{b*}) by

$$s_{b*} = \frac{Z_S^*}{X_S^*} s_b. \tag{16}$$

It is obvious that the slope s_{b*} is dimensionless, but the subscript ''*'' is intended to indicate that such slope is based on the real dimensional domain. The dimensionless formulation indicates that if one obtains results of water and solute transport in a beach, these results would represent other beaches (with the geometry given in Fig. 1) provided the following parameters are kept the same: M, α, the dimensionless tidal period $T = \frac{T^*}{T_s^*}$, and D_f. The remaining parameters, such as porosity ϕ, and the van Genuchten parameter ''n'' play a minor role as our previous works (Boufadel, 2000; Naba et al., 2002; Li et al., 2007a). Recall that as the domain gets taller, conservation of the value of α requires a porous medium that is more fine-textured. Thus, the dimensionless formulation shows that a necessary condition for hydraulic similarity between a tall domain and a short one is that the latter is more coarse-textured than the prior in a way that the quantity $\alpha = \alpha^* Z_S^*$ is conserved. This should be accounted for when designing experiments in laboratory sand flumes.

Based on (10), by varying M one can use a dimensionless domain with a beach slope s_b to simulate dimensional (real) beaches with different slopes s_{b*}. This is done herein, using a dimensionless beach domain with $L_x = 80$, $L_z = 5$ and $s_b = 0.1$.

Boundary and initial conditions

The boundary and initial conditions will be given directly in terms of the dimensionless form. As one moves inland, the water table tends to rise due to recharge from rainfall. Thus, at a sufficiently large distance from the beach, the water table will reach eventually the elevation of the high tide, which is 4.0 herein. Therefore, the landward boundary condition is

$$\psi|_{x=0} = 4 - z, \quad \text{if } z \leqslant 4, \tag{17}$$

$$c^*|_{x=0} = 0, \quad \text{if } z \leqslant 4. \tag{18}$$

On the beach surface, a seepage face was allowed to develop. (Note that the pressure of the seepage face is equal to zero and the water flow is outward). Seaward of the seepage face, the pressure on the submerged beach surface was obtained based on the tide level: $\psi|_{\text{beach surface}} = \beta_{sea}[h_{sea}(t) - z]$, where $\beta_{sea} = 1.02$, because the salt concentration at sea was taken as 32.0 kgm^{-3}, typical at the coasts of the continental USA (Wrenn et al., 1997); $h_{sea}(t) = h_{sea}^*(t)/Z_S^*$ is the dimensionless tidal level. No-flow boundary condition is used on the reminder boundaries.

The concentration boundary condition depended on the water flow sense. At locations where seawater is entering the beach, the salt concentration was set equal to that of the sea (32 kgm^{-3}). Otherwise, an outflowing boundary condition was adopted, where the water leaves the beach without a change in concentration (i.e., a zero dispersive flux). This is an approach adopted in previous works (Galeati et al., 1992; Boufadel, 2000; Li et al., 2007a).

The initial conditions were a hydrostatic pressure distribution under a high tide with a zero concentration within the domain. These are arbitrary but physical conditions. The simulations were conducted for long enough time such that the solutions became periodic in time, eliminating therefore any errors that would result from the choice of the initial conditions.

Model parameter analysis

One of the advantages of the dimensionless model is that it has less independent model parameters. In order to further reduce the independent model parameters, we set $Z_S^* = A^*$, the tidal amplitude. This choice is arbitrary depending on the system under consideration. For example, one would set Z_S^* equal to the wave amplitude (or runup) if one is investigating the effects of waves (say in the absence of tide). From Eq. (16) and $Z_S^* = A^*$, the horizontal characteristic scale is given by $X_S^* = A^* s_b / s_{b*}$. From Eq. (8), the dimensionless tidal period is

$$T = \frac{T^*}{TS^*} = \frac{T^* K_0^*}{A^*} \tag{19}$$

and the dimensionless tidal level is

$$h_{sea}(t) \overset{\text{def.}}{=} h_m + \cos\left(\frac{2\pi}{T} t\right), \tag{20}$$

where h_m is the ratio of the mean sea level to the tidal amplitude. By setting $h_m = 3.0$, the dimensionless tidal level fluctuates between the elevations 2.0 and 4.0.

Given the dimensionless domain with $s_b = 0.1$, $L_x = 80$ and $L_z = 5$, the goal is to determine the numerical solution of the dimensionless model (9)–(18), which requires knowledge of the values of the following eight parameters:

$$\{s_{b*}, T, \phi, n, S_r, h_m, \alpha, D_f\}. \tag{21}$$

To convert a dimensionless numerical solution into a dimensional solution, one needs two other parameters A^* and T^*, which satisfy (19). Table 1 lists the relationships of the physical quantities for the dimensional and dimensionless domains. By choosing suitable but different values of the auxiliary parameters A^* and T^*, one dimensionless result (or solution) can be interpreted as different results of various dimensional configurations with different values of A^* and T^* provided that Eq. (19) is satisfied.

Table 1 Relationships of parameters in the dimensional and dimensionless models

L_z^*	L_x^*	dF^*	dF_c^*	K_0^*	h_m^*	α^*	D_f^*
$A^* L_z$	$\frac{A^* L_x s_b}{s_{b*}}$	$A^* K_0^* \frac{s_b}{s_{b*}} dF$	$A^* K_0^* \frac{s_b}{s_{b*}} dF_c$	$A^* \frac{T}{T^*}$	$h_m A^*$	αA^*	$\frac{D_f T^*}{A^{*2} T}$

(The two terms in each column are identical. Terms in the first row are dimensional parameters, and terms in the second row are combinations of the dimensionless parameters and the two dimensional parameters A^* and K_0^*).

The beach slope of the real domain is modified in numerical simulations by adjusting the values of the parameter M, which is defined as Eq. (10) and included in the model governing Eqs. (9) and (12). The permeability, tidal period and amplitude are grouped into one dimensionless parameter T in the dimensionless model. This means that for the dimensionless formulation, the effects of changes in permeability, tidal period and tidal amplitude on the dimensionless solution will be the same as long as they lead to the same value of T. For example, consider two tidal beaches with same slopes and tidal amplitudes, one is characterized by diurnal sea tide and a permeability of 1 m/h, while the other by semidiurnal sea tide and a permeability of 2 m/h. These two beaches lead to the same value of T and therefore have the same dimensionless model. The unique dimensionless solution of the same model can be converted into individual, different dimensional solutions for each of the two systems using the transform formula listed in Table 1. In application, the tidal period T^* can be semidiurnal (12.25 h) or diurnal (24.8 h), using the expression of K_0^* in terms of T^*, A^* and T in Table 1, any value of K_0^* can be realized by setting suitable value of T. The variable ranges for various parameters are reported in Table 2.

Numerical simulations

The MARUN (for MARine UNsaturated) model (Boufadel et al., 1999b) is used herein. The model can simulate transient and steady seepage faces according to the standard approach reported by Neuman (1973), Pinder and Gray (1977). The MARUN code was verified extensively in the literature (Naba et al., 2002) and validated by reproducing previous well-known numerical results such as the Henry's problem of seawater intrusion (Frind, 1982; Croucher and O'Sullivan, 1995) and the Elder problem (Elder, 1967) by Boufadel et al. (1999b,d).

The beach domain was discretized into a mesh with 30,651 nodes and 60,000 triangular elements. The mesh was relatively fine near the beach surface (triangles with length of 0.1 and height of 0.02–0.04), and became gradually coarse toward the left boundary. At that location, the largest height of the triangular elements was 0.16 and the largest length was 0.26. The elevation difference of two adjacent nodes on the beach surface was 0.01. Because the simulations started at high tide, the time step was set to be:

$$\Delta t = \begin{cases} \frac{T}{2\pi}\{\arccos[h_{sea}(t_{old}) - h_m - 0.01] - \arccos[h_{sea}(t_{old}) - h_m]\} & \text{for falling period,} \\ \frac{T}{2\pi}\{\arcsin[h_{sea}(t_{old}) - h_m + 0.01] - \arcsin[h_{sea}(t_{old}) - h_m]\} & \text{for rising period,} \end{cases} \quad (22)$$

where t_{old} is the time in the last time step. Such a choice of the time step ensured that the sea level changed a constant distance of 0.01 in each time step, matching therefore the nodes on the beach surface. This technique was adopted to avoid formation of a ''numerical'' seepage face, which would occur if the sea level were between two consecutive nodes. As a result, 400 time-steps were used for each tidal cycle. The convergence criterion of the Picard iteration was set at 10^{-5}, and such value was arrived at after we noticed that the solutions are unchanged for smaller values of the convergence criterion. Numerical simulation using refined mesh gave the same salinity and pressure distributions, indicating that the mesh used is fine enough.

Results

The parameter M took the following five different values (M = 0.1, 0.25, 1.0, 4.0, and 10.0) corresponding to the following dimensional slopes: s_{b*} = 0.0316, 0.05, 0.1, 0.2, 0.316. Two dimensionless tidal periods were considered: T = 4.41 and T = 44.1. The remaining parameters were kept at the following values:

$$(\phi, n, S_r, h_m, \alpha, D_f) = (0.3, 3.0, 0.01, 3.0, 10, 0.01).$$

The value of D_f indicates a small dispersion, which would occur in homogeneous material, where pore scale variability causes dispersion. Considering that sandy beaches are relatively homogeneous, the assumption of small dispersion coefficient is plausible.

Transient distributions of salinity and Darcy velocity

Fig. 3 of Li et al. (2007a) shows ''snapshots'' of the beach at various times for a dimensional beach slope s_{b*} = 0.316 and a dimensionless tidal period of 4.41. The high salinity occupies the top portion of the intertidal zone and is underlain by low salinity, which pinches out near the low-tide line. This was demonstrated by Boufadel (2000) and recently reproduced numerically by Robinson et al. (2007). In many studies, a saltwater wedge forms seaward of the low tide line (Ataie-Ashtiani et al., 1999a; Werner and Lockington, 2006). This was not the case in this study due to the shallow depth of the aquifer that resulted in high seaward fresh groundwater flow that washed the saltwater (and a potential wedge) to sea.

The situation when (s_{b*}, T) = (0.1, 4.41) was reported in Fig. 2. A comparison between the two cases when (s_{b*},

Table 2 Value ranges of the length, height and beach slope of the dimensional domains represented by the dimensionless domain in Fig. 1 for reasonable and numerically applicable values of A^*, s_{b*}

s_b	L_x	L_z	A^* (m)	s_{b*}	L_x^* (m)	L_z^* (m)
10%	80	5	0.3–2	3.16–31.6%	7.59–506	1.5–10

T) = (0.316, 4.41) and (0.1, 4.41) illustrates the role of the slope, as all other quantities of interest are the same. The salinity contours in Fig. 2 ''touched'' the bottom, while they were ''hanging'' in the intertidal zone when (s_{b*}, T) = (0.316, 4.41). For the same slope as in Fig. 2 but for a large period ($s_{b*} = 0.1$, $T = 44.1$), the salinity contours are more landward than those of Fig. 2, as shown in Fig. 3. For the same dimensionless tidal period as in Fig. 3 but

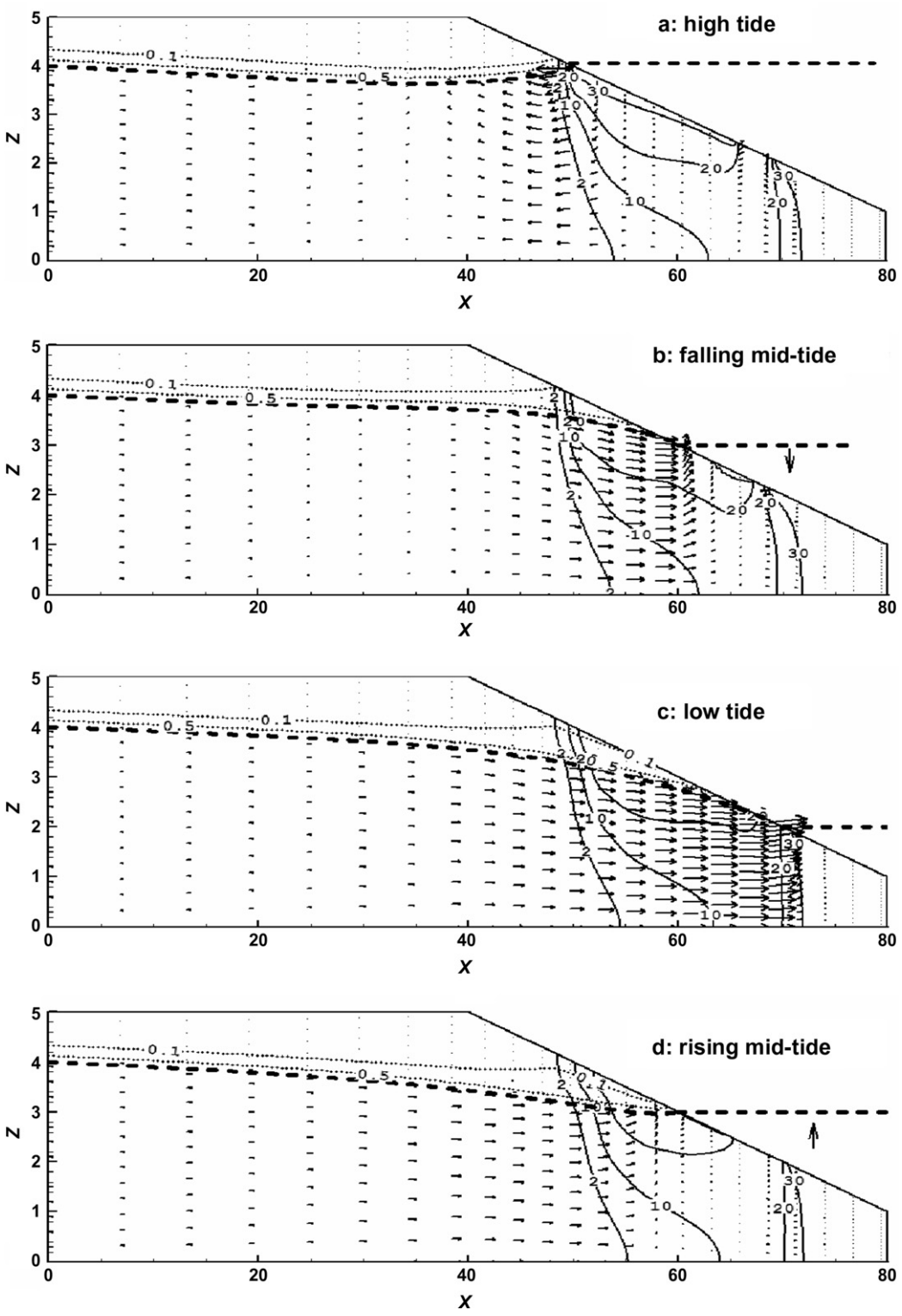

Figure 2 Salinity (in kgm^{-3}), the velocity field, and degree of water saturation when (s_{b*}, T) = (0.1, 4.41) at four different times. The thin lines represent the salinity. The arrows represent the Darcy flux. The dotted lines represent the degree of water saturation. The dashed lines represent the beach water table and the sea water level.

for a smaller slope (s_{b*} = 0.0316, T = 44.1), Fig. 4 shows that the salinity contours even more landward than those of Fig. 3. Figs. 2 and 4 have the same length scale for the Darcy velocity, which is 4 times of that in Fig. 3.

Two major factors could have affected the salinity distributions. These are the location of the water table in the intertidal zone and the exchange flows of the beach (with the inland aquifer and with the sea). The effects of the water table will be investigated by analyzing the transient seepage as conducted next.

The following observations and conclusions can be made from Figs. 2, 3, 4 and Fig. 3 of Li et al. (2007a): (1) The maximum Darcy velocity always occurs at the intersection of the watertable and the beach surface. The magnitude of the Darcy velocity in offshore beach (i.e., the beach area seaward of the low tide line) is much smaller than that in

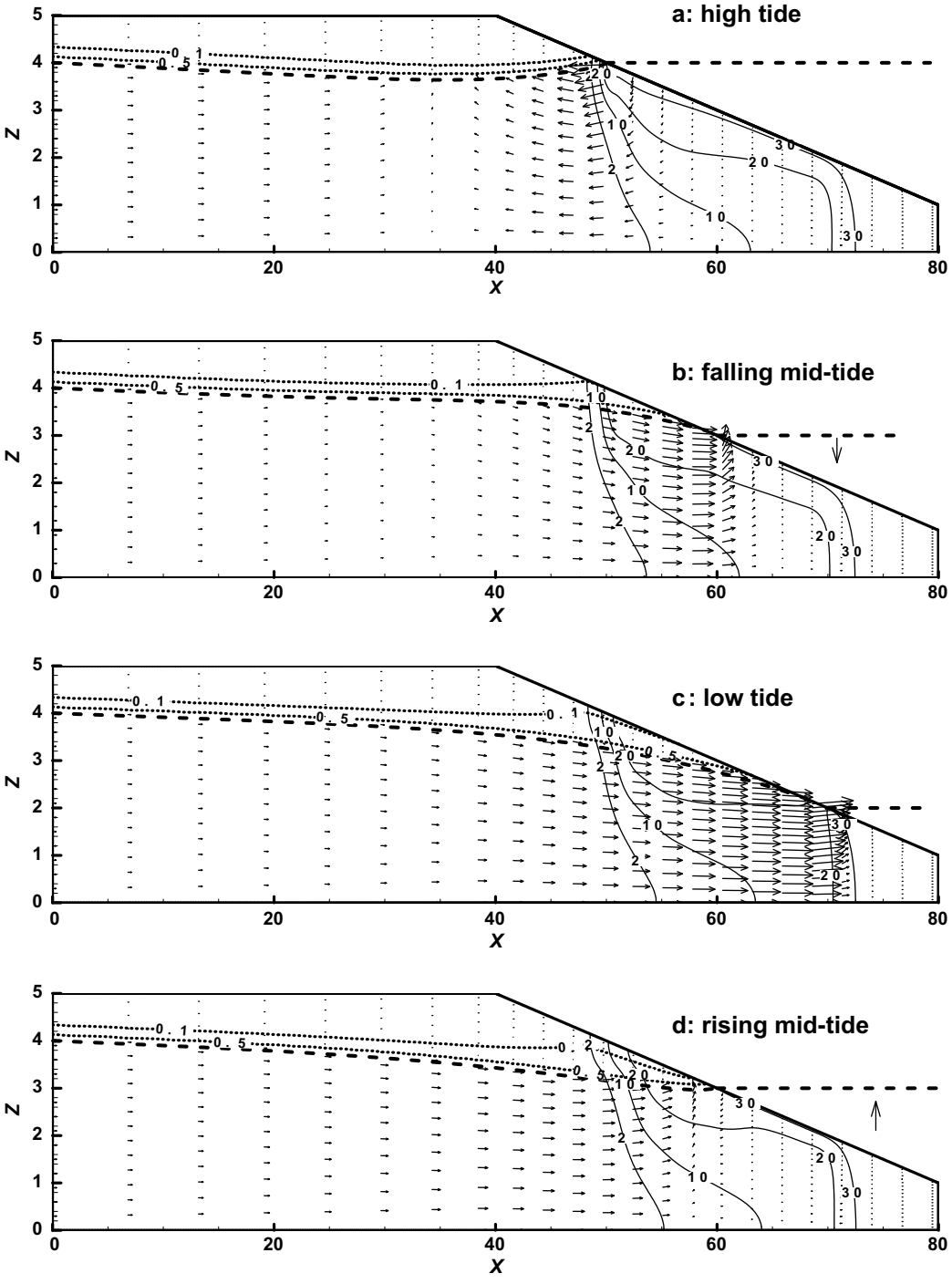

Figure 3 Salinity (in kgm^{-3}), the velocity field, and degree of water saturation when (s_{b*}, T) = (0.1, 44.1) at four different times. The thin lines represent the salinity. The arrows represent the Darcy flux. The dotted lines represent the degree of water saturation. The dashed lines represent the beach water table and the sea water level.

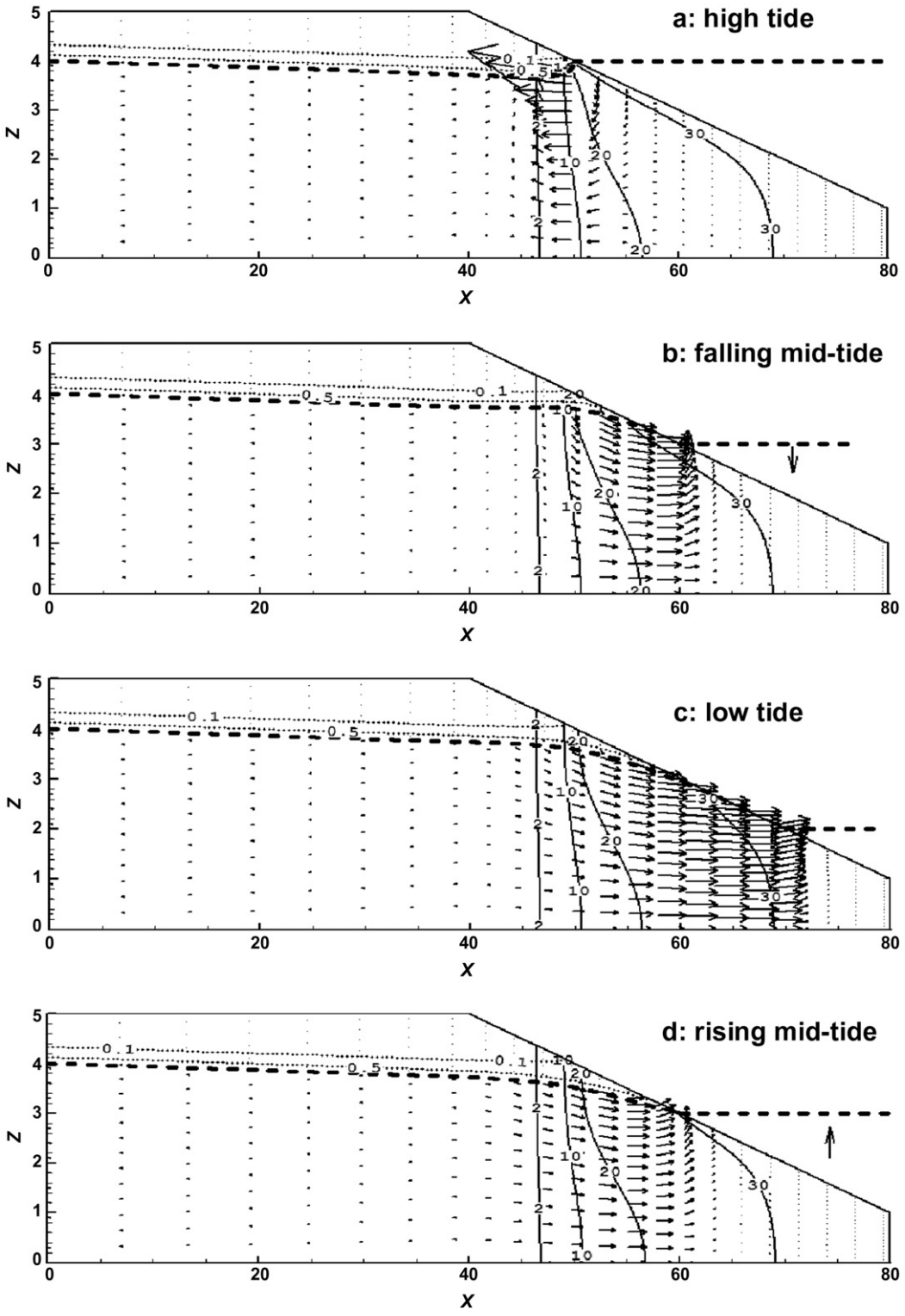

Figure 4 Salinity (in kgm^{-3}), the velocity field, and degree of water saturation when (s_{b*}, T) = (0.0316, 44.1) at four different times. The thin lines represent the salinity. The arrows represent the Darcy flux. The dotted lines represent the degree of water saturation. The dashed lines represent the beach water table and the sea water level.

onshore area (i.e., the domain landward of the low tide line), indicating that the offshore groundwater is almost stagnant compared with the onshore groundwater flow. These simulation results may explain the previous observations (Bokuniewicz, 1980; Cable et al., 1997; Taniguchi, 2002; Slomp and Van Capellen, 2004; Taniguchi et al., 2006) that the major portion of the seaward groundwater seepage usually occurs in the shallow part of the submerged

beach and that the magnitude of the seaward groundwater seepage decreases with seaward distance away from the coast. (2) The periodic tidal submersion forms saltwater plumes beneath the beach surfaces. Smaller beach slope or inland freshwater recharge, or greater beach permeability may lead to larger salt plume. In some cases, the freshwater discharge path disappears. In the extreme case that there is no inland freshwater recharge (i.e., no-flow boundary condition on the left boundary), the salt plume will occupy the whole beach area, and ultimately, there will be no fresh water in the whole domain considered.

Using the parameter relationships given in Table 1, the dimensionless results in Fig. 3 of Li et al. (2007a) and Fig. 2 here (where T is fixed at 4.41) can be interpreted as results for various dimensional systems with different tidal amplitude, period and beach permeability which satisfy

$$K_0^* = A^* \frac{T}{T^*} = \frac{4.41A^*}{T^*}, \tag{23}$$

where T^* = 12.25 h or 24.5 h and A^* represents the tidal amplitude. For example, the results corresponding to T = 4.41 can represent a tidal beach system of A^* = 2.0 m, $K_0^* = 2\times10^{-4}$ m/s with semidiurnal tides (T^* = 12.25 h), or a tidal beach system of A^* = 0.3 m, $K_0^* = 1.5\times10^{-5}$ m/s with diurnal tides (T^* = 24.5 h). Consequently, one dimensionless simulation results can be used to represent tidal beach systems with A^* = 0.3 m–2.0 m, $K_0^* = 3\times10^{-5}$ m/s–2×10^{-4} m/s for semidiurnal tides (T^* = 12.25 h) and 1.5×10^{-5} m/s–1.0×10^{-4} m/s for diurnal tides (T^* = 24.5 h) as long as they satisfy Eq. (23).

Similarly, when T = 44.1 as in Figs. 3 and 4, the hydraulic conductivity K_0^* varies from 3×10^{-4} m/s to 2×10^{-3} m/s for semidiurnal tides (T^* = 12.25 h) and from 1.5×10^{-4} m/s to 1×10^{-3} m/s for diurnal tides (T^* = 24.5 h) as A^* ranges from 0.3 m to 2.0 m. The above K_0^* values cover the value range of the hydraulic conductivity K_0^* for the typical beach soils.

Seepage face

Fig. 5 reports variation of the seepage face height within the tidal cycle, as function of the dimensionless tidal period and slope of the real beach s_{b*}. One can see that the seepage face reaches its maximum height at low tide and vanishes near the high tide for all cases. For a given slope, the maximum values occurred for the smaller dimensionless tidal period, T = 4.41. This can explained based on the definition of the dimensionless period, $T = \frac{T^* K_0^*}{A^*}$, if T^* is given (say 12.25 h, semi-diurnal tide), smaller T means smaller hydraulic conductivity of the beach material or a larger amplitude of tidal fluctuation. In both cases, the seepage face would be large. For a given value of T, the height of seepage face increased as the beach slope s_{b*} decreased. These results are consistent with the numerical results of Naba et al. (2002) where the height of the transient seepage face of trapezoidal domains (a finite slope) was consistently larger than that of rectangular domains (infinite slope). It is related to the reduction of drainage ability of the beach as the beach slope decreases. This will be elaborated on later.

A major observation in Fig. 5 is that the curves corresponding to T = 4.41 appear symmetric with respect to t = 0.5, while those corresponding to T = 44.1 are skewed to the left (higher in the first half of the tidal cycle). This could be explained as follows: For the fast tide (T = 4.41), the water table dynamics near the beach surface is separated from the rest of the domain due to the rapid movement of the sea level. In such a situation, the movement of the water table is dictated by the drainage of the pores. For the slow tide (T = 44.1), there is sufficient time for replenishment of the beach from the landward side, causing the height of the seepage face during rising tides to be smaller than that during falling tides. The notion of separation of water table hydraulics from the rest of the domain was first introduced by Dracos (1963). The publication is in German though, and a good discussion on it was provided by Turner (1993). Naba et al. (2002) analyzed the problem while accounting for capillary forces, and found that the higher the static capillary fringe (inverse of α) the earlier the separation occurs. Investigation of the effects of capillary forces is left for future work.

Exchange flows

The selection of the Dirichlet boundary condition landward of the beach subsumes that the landward water table is ''far enough'' from the beach such it is not affected by the tidal fluctuations. To test our assumption, we conducted simulations where a no-flow Neumann boundary condition was adopted at x = 0. We found that the water table at x = 0 was unaffected by the tide for all situations except for T = 44.1 and $s_{b*} \geqslant 0.2$. Thus, a Dirichlet boundary condition is not appropriate for those latter situations. And for consistency, the results are not reported for T = 44.1 and $s_{b*} \geqslant 0.2$.

We compute in what follows the inflow volumes to the beach through three regions: The left boundary, the beach surface below the low tide line, and the beach surface above the low tide line. We also compute the cumulative outflow volumes through the beach surface below the low tide line and the beach surface above the low tide line. The outflow volume through the seepage face is reported as a portion of the beach surface above the low tide line. Let V_{in}^* and V_{out}^* be the designations of the dimensional inflow and outflow volumes over a tidal cycle, respectively. It can be shown that the relations with their dimensionless counterparts are:

$$\frac{V_{in}^*}{(A^*)^2} = \frac{V_{in}}{\sqrt{M}} = \frac{s_b V_{in}}{s_{b*}} = \frac{0.1 V_{in}}{s_{b*}}, \tag{24}$$

$$\frac{V_{out}^*}{(A^*)^2} = \frac{V_{out}}{\sqrt{M}} = \frac{s_b V_{out}}{s_{b*}} = \frac{0.1 V_{out}}{s_{b*}}, \tag{25}$$

where the fact that s_b = 0.1 is used in the last equalities.

Fig. 6 reports $V_{in}^*/(A^*)^2$ as function of the beach slope s_{b*} for T = 4.41 (Fig. 6a) and T = 44.1 (Fig. 6b). The results are shown for the two types of boundary conditions at x = 0: Dirichlet (i.e., water level is 4.0 at x = 0) and no-flow Neumann (i.e., impermeable wall at x = 0). For the Dirichlet boundary condition, the inflow volume (of freshwater) through the left wall increased with the beach slope for both dimensionless periods. Groundwater flow is more or less inversely proportional to the length of the system (along the flow), which is L_x^*. However, such a value is inversely proportional to the slope of the physical beach

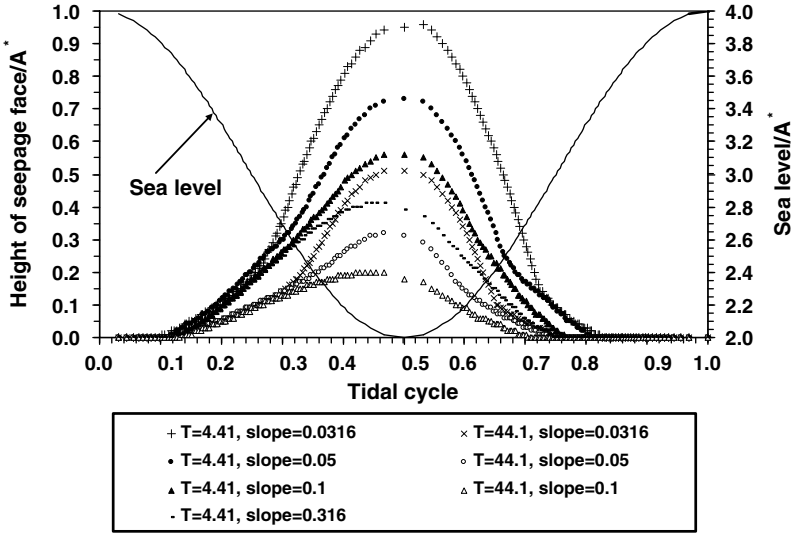

Figure 5 Changes of the heights of the seepage faces with the dimensionless time (in tidal cycle) for different values of s_{b*} and T.

($L_x^* = A^* L_x \frac{s_b}{s_{b*}}$). Therefore, one may understand how the inflow to the beach through the left boundary is directly proportional to the slope s_{b*}.

The inflow volume from the sea through the beach surface below the low tide line increased with the slope. But it was essentially negligible, and is not expected to affect

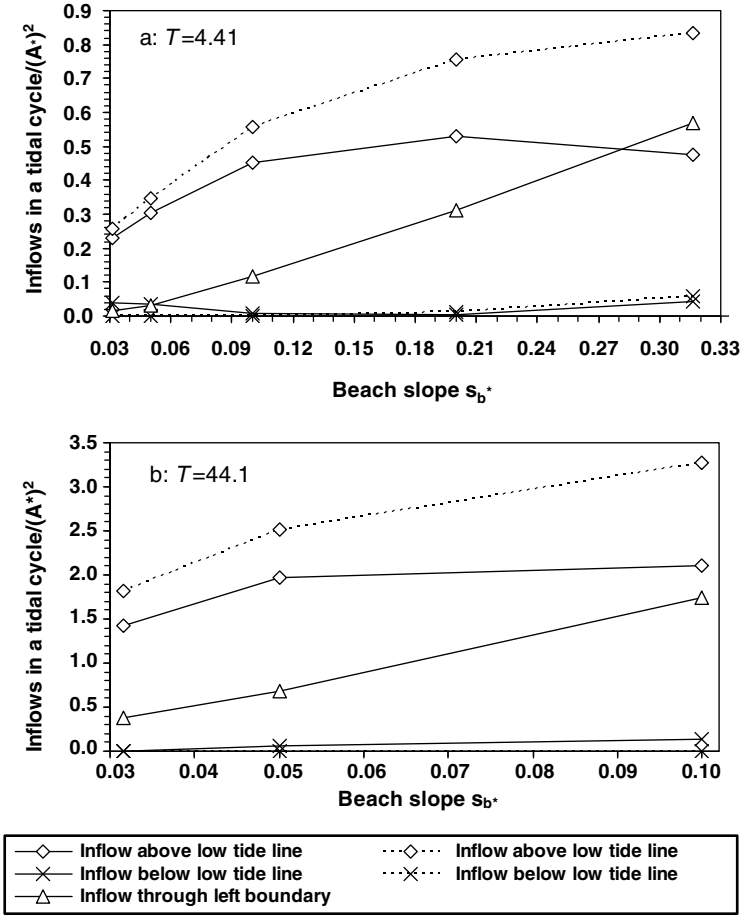

Figure 6 Changes of the inflows from different boundary parts in a tidal cycle with the beach slope s_{b*} when the dimensionless tidal period T is fixed at (a) 4.41 and (b) 44.1. The thick solid lines are results when there are inland freshwater recharges specified by Dirichlet boundary condition (17). The thin dashed lines are results when no-flow Neumann boundary condition was used at the left boundary.

the salinity distribution in the beach. However, such an inflow might play an important role in chemical transformation in the beach due to difference in chemical composition between seawater and beach water stagnating seaward of the low tide line. Examples of interest include nutrients that are usually absent from pristine beaches but abundant at sea during upwelling seasons (Eslinger et al., 2001).

The inflow volume from the sea through the beach surface above the low tide line did not behave in a monotonic way. Rather it displayed maximum values at $s_{b*} = 0.2$ and 0.05 for $T = 4.41$ and 44.1, respectively. The results for $T = 44.1$ are approximately one order of magnitude greater than those for $T = 4.41$, indicating that the inflow above the low tide line in a tidal cycle increases with the beach permeability K_0^* because the dimensionless tidal period T is proportional to $K_0^*(T = T^* K_0^*/A^*)$.

For the cases without inland recharges (thin dashed lines with diamond symbols), Fig. 6 shows that the inflow above the low tide line increases with s_{b*}. The decrease of the beach slope can reduce the drainage speed of the beach pore water as the tide falls. In this case less pore space is emptied out for infiltration as the tide rises (e.g., at the extreme case of flat beach surface, the soil becomes always saturated and no infiltration happens as the tide rises). Therefore, extremely small beach slope will lead to small inflow in the intertidal zone in a tidal cycle.

When there are inland recharges (thick solid lines with diamond symbols), the inflow in the intertidal zone is no longer monotone with respect to s_{b*} due to the effect of the inland freshwater recharge, which will enhance the watertable and reduces the pore space in the intertidal zone. Consequently, large inland recharge results in small inflow into the intertidal zone. The thin dashed curve with diamond symbols is always above the thick solid curve with diamond symbols both in Figs. 6a and b, indicating that the inflow in the intertidal zone without inland recharge is greater than that with inland recharge. That is to say, the inland recharge can significantly damp the seawater volume of the tide-induced seawater–groundwater recirculation in the intertidal zone. This is in line with the numerical simulation results of Prieto and Destouni (2005) (Fig. 4 of their paper) and of Robinson et al. (2007) (Fig. 9 of their paper).

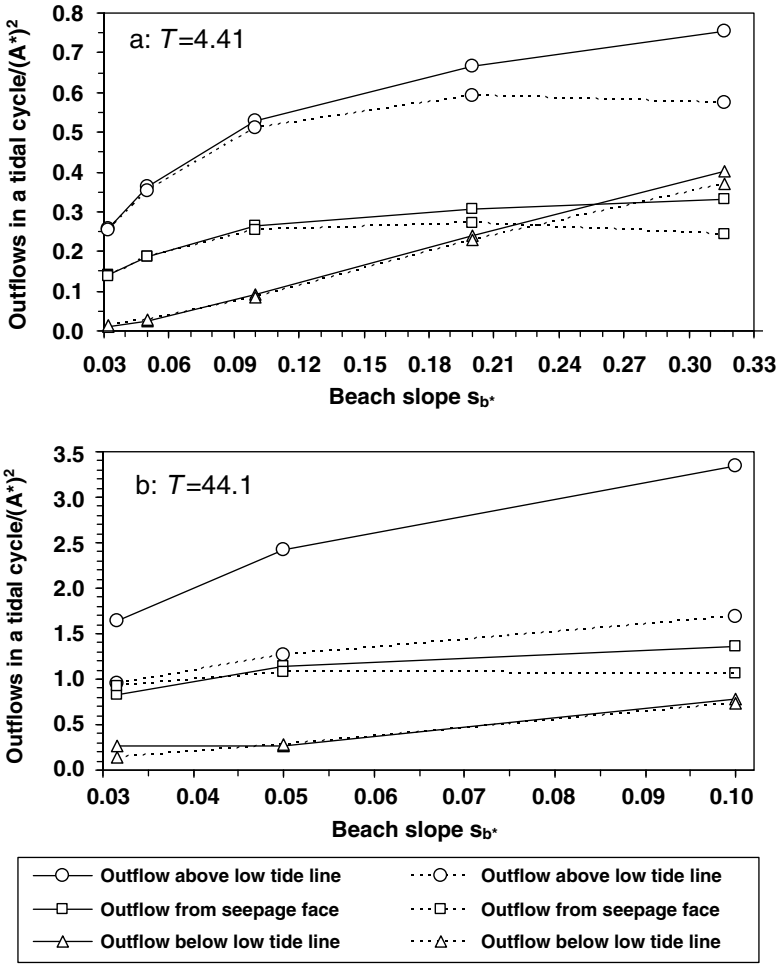

Figure 7 Changes of the outflows from different boundary parts in a tidal cycle with the beach slope s_{b*} when the dimensionless tidal period T is fixed at (a) 4.41 and (b) 44.1. The thick solid lines are results when there are inland freshwater recharges specified by Dirichlet boundary condition (17). The thin dashed lines are results when no-flow Neumann boundary condition was used at the left boundary.

Fig. 7 reported $V^*_{out}/(A^*)^2$ as function of the beach slope s_{b*} for $T = 4.41$ (Fig. 7a) and $T = 44.1$ (Fig. 7b). The outflow above the low tide line includes that through the seepage face, which is also shown to assess the importance of seepage flow. The following observations and discussions can be made:

Obviously, the outflows above the low tide line with inland freshwater recharge are greater than those without inland recharge. Their difference is small when both T and s_{b*} are small. This is because small T and s_{b*} lead to small inland recharge, almost zero. The differences between the outflows through the seepage face with and without inland recharge are small for all the cases (the solid and dashed curves with squares).

The outflow from the seepage face accounted for 41–97% of the outflow through the intertidal zone (average 55%), and 26–85% (average 46%) of the whole outflow (by including the outflow from beneath the low tide line) through the right boundary. This indicates that the outflow through the seepage face is not negligible as implicitly assumed in studies that neglected the seepage face. A detailed comparison of the current numerical results with those that neglect the seepage face is therefore an interesting work in the future. The differences between the outflows below the low tide line with and without inland recharge are small for all the cases (the solid and dashed curves with diamond) and increases with the beach slope.

Comparisons with previous studies

Based on field observations, Colbert (2004) obtained an estimation of 1.0 ± 0.3 m^3 day^{-1} m^{-1} for the inflow through the intertidal zone of a beach at the head of Catalina Harbor, CA. The beach slope is about 0.045 and falls in the range of the simulation results in our paper. The diurnal tidal amplitude was about 0.8 m. So a rough estimation of the inflow in the intertidal zone can also be made simply based on our simulation results in Fig. 6. In fact, the dimensionless inflow into the intertidal zone (i.e., above the low tide line) for $s_{b*} = 0.045$ ranged from $\sim$0.3 (solid line with diamond when $T = 4.41$ in Fig. 6a) to $\sim$2.3 (thin dashed line with diamond at $T = 44.1$ in Fig. 6b). Using these data, the inflow in the intertidal zone should range from the minimum of $0.3 \times 0.8^2 = 0.192$ m^3 day^{-1} m^{-1} to the maximum of $2.3 \times 0.8^2 = 1.472$ m^3 day^{-1} m^{-1}. These lower and upper bounds include Colbert's (2004) field observation of 1.0 ± 0.3 m^3 day^{-1} m^{-1}, in view of the wide value ranges of the beach permeability and slopes considered in the numerical simulations here.

For typical diurnal tides with amplitude of 0.65 m used by Prieto and Destouni (2005), using data in Fig. 6, the minimum inflow in the intertidal zone is $0.23 \times 0.65^2 \times 365 = 35.5$ m^3 yr^{-1} m^{-1}, and the maximum inflow in the intertidal zone is $3.28 \times 0.65^2 \times 365 = 505.8$ m^3 yr^{-1} m^{-1}. Prieto and Destouni (2005) obtained a maximum total inflow of about 2000 m^3 yr^{-1} m^{-1} (including the inflow under the low tide line) for very deep coastal aquifers (50-150 m). They did not provide the inflow data in the intertidal zones separately. Therefore, it may be concluded that the inflow below the low tide line of the very deep aquifers considered by them accounts for the major portion of the total inflow. Here, however, due to the shallow depth of the considered domains, the inflows below the low tide line are much smaller than that above the low tide line, and can even be neglected when conducting water balances for all the simulated cases.

Robinson et al. (2007) considered a beach aquifer system with a depth of 30 m and total length of 200 m (inland length 150 m). The inland freshwater recharge (Q_f in their paper) used in their simulations ranged from 0.3 m^2/d to 4.3 m^2/d. Dividing Q_f with the depth of 30 m, the recharge flux on their left boundary ranges from 0.01 to 0.1433 m/d. They obtained inflow above the low tide line ranging from 0.82 m^2/d to 7.47 m^2/d (see the ''Tidally driven inflow (m^2/d)'' in Table 1 of their paper). The model parameter values of their beach aquifer are: beach slope = 0.1, beach hydraulic conductivity = 10 d/m, tidal period = 12 h, and tidal amplitude = 0.5, 1 and 2 m. Using the definition $T = T^* K_0^*/A^*$, the dimensionless tidal period for their model is $T = 2.5$, 5, and 10. Because our simulations only have two $T-$ values (4.41, 44.1), their results can be compared only roughly with ours in Fig. 6a where $T = 4.41$. When the beach slope is 0.1, the inland recharge in Fig. 6a ranges from 0 (no-flow Neumann boundary condition, not shown) to 0.1186 A^{*2} per tidal cycle, corresponding to a inland recharge flux of 0–0.1186 m/d (using the data $A^* = 2$ m, and tidal period =0.5 day), and the inflow above the low tide line ranges from 0.4536 A^{*2} to 0.5553 A^{*2} per tidal cycle, or equivalently from 0.227 m^2/d to 4.44 m^2/d (using the data $A^* = 0.5$, 1, and 2 m, and tidal period = 0.5 day). Thus, the inflow above the low tide line in our paper is a little bit smaller than those by Robinson et al. (2007). The discrepancy may be caused by the difference of the parameter T (our is 4.41, and theirs are 2.5, 5 and 10), and most probably by neglecting of the seepage face in their model because the inflow will be significantly ''blocked'' by the seepage face when the tidal level is near the low tide line. The relatively slight difference seems to indicate that the influence of the aquifer's depth on the inflow above the low tide is very limited.

Summary

This paper investigated the groundwater–seawater circulations in beaches driven by tides. Rigorous evaluation of the hydraulics of such systems requires understanding density-dependent flows in variably-saturated media and incorporating important factors such as the inland recharge, the beach slope, seepage face, soil permeability, unsaturated zone, capillary effects, the density-and-viscosity-effects of the salt transport, and the tidal amplitude and period. We conducted the numerical simulations using the finite element model MARUN (Boufadel et al., 1999a) by introducing a dimensionless formulation that allowed generalization of the simulation results. The real beach domains with typical slope values (3.16–31.6%) were transformed into one dimensionless domain with a slope of 10% by using suitable horizontal and vertical scaling. The slope of the real beach domain appears only in the flow and solute transport equations for the dimensionless model. The dimensionless formulation avoided the finite element aspect ratios that are too small to guarantee adequate accuracy for numerical solutions of beach domains with extremely small slopes.

From a dimensionless tidal period and a dimensionless beach slope, we obtained results that apply to a wide range of beach permeabilities and/or slopes with corresponding inland freshwater recharge specified by a fixed boundary watertable.

The numerical simulations demonstrated the following important facts: The maximum Darcy velocity always occurs at the intersection of the watertable and the beach surface. The offshore beach groundwater is almost stagnant compared with the onshore groundwater flow, which may explain the previous observations (Bokuniewicz, 1980; Cable et al., 1997; Taniguchi, 2002; Slomp and Van Capellen, 2004; Taniguchi et al., 2006) that the major portion of the seaward groundwater seepage usually occurs in the shallow part of the submerged beach and that the magnitude of the seaward groundwater seepage decreases with seaward distance away from the coast. On the average, the outflow from the seepage face accounts for about half the outflow from the intertidal zone. The seawater infiltrating into the intertidal zone in a tidal cycle increases with the beach permeability, and decreases when the inland recharge increases. The periodic seawater submersion of the beach forms a saltwater plume in the beach. Smaller beach slopes, smaller inland freshwater recharges, and/or greater beach permeability lead to larger salt plumes. The inflows in the intertidal zones range from 35.5 $m^3\,yr^{-1}\,m^{-1}$ to 505.8 $m^3\,yr^{-1}\,m^{-1}$ for all the cases considered. The numerical results are in line with field and laboratory experiment observations by previous researches, in particular, with the recent important field observation-based estimations of the tide-induced submarine groundwater discharge in the intertidal zone.

Acknowledgements

Funding for this work was provided by the US Department of Environmental Protection. However, no official endorsement should be inferred. This research is also partially supported by the National Natural Science Foundation of China (No. 40672167).

Appendix. List of notations

A^* [L] tidal amplitude

c^* [ML^{-3}] salt concentration of the aquifer pore water

D_f^* [L^2T^{-1}] & D_f dimensional and dimensionless dispersion coefficients, respectively

dF the dimensionless Darcy flow rate through the arc ds in the dimensionless domain

dF^* [L^2T^{-1}] the Darcy flow rate through the arc ds^* in the dimensional domain. $\frac{dF^*}{Z_S^* K_0^*} = \frac{dF}{\sqrt{M}}$

h_m^* [L] & h_m [−] dimensional and dimensionless mean sea levels, respectively

h_{sea}^* [L] & h_{sea} [−] dimensional and dimensionless sea levels, respectively.

K_0^* [LT^{-1}] saturated freshwater hydraulic conductivity of beach soil

$k_r(S)$ relative permeability for given water saturation S

L_x^* [L] & L_x horizontal lengths of the dimensional and dimensionless domains, respectively

L_z^* [L] & L_z vertical heights of the dimensional and dimensionless domains, respectively

m and n soil parameters of the van Genuchten (1980) model ($m = 1 - (1/n)$)

M model transform parameter, $M = (Z_S^*/X_S^*)^2 = (s_{b*}/s_b)^2$

$\mathbf{q}^* = (q_x^*, q_z^*)$ dimensional Darcy flux (the dimension of its component is [LT^{-1}])

$\mathbf{q} = (q_x, q_z)$ dimensionless Darcy flux, $\mathbf{q}^* = (K_0^* A^* s_b/s_{b*})\mathbf{q}$

s_{b*} & s_b beach slopes of the dimensional and dimensionless domains, respectively

S degree of water saturation (fraction of pore volume occupied by water)

S_e effective degree of water saturation (normalized water saturation $S_e = (S - S_r)/(1 - S_r)$)

S_r residual soil water saturation

t^*[T] & t dimensional and dimensionless time variables, respectively

T^* [T] & T dimensional and dimensionless tidal periods, respectively

T_S^*[T] the characteristic time scale, $T_S^* = Z_S^*/K_0^*$

x^* [L] & x dimensional and dimensionless horizontal coordinates, respectively

X_S^* [L] characteristic scale in horizontal direction

z^*[L] & z dimensional and dimensionless vertical coordinates, respectively

Z_S^* [L] characteristic scale in vertical direction

α^* [L] & α dimensional and dimensionless parameters of the van Genuchten (1980) model for describing the soil capillary effects

β ratio of saltwater density to freshwater density

δ ratio of freshwater dynamic viscosity to saltwater dynamic viscosity

ε^* [L^3M^{-1}] fitting parameter ($6.46 \times 10^{-4}\,m^3\,kg^{-1}$) for the concentration–density curve

ξ^* [L^3M^{-1}] fitting parameter ($1.566 \times 10^{-3}\,m^3\,kg^{-1}$) for the concentration–dynamic viscosity curve

μ^* [$ML^{-3}T^{-1}$] & μ_0^* [ML^{-3}] dynamic viscosity of the beach pore water and the freshwater at 20 °C, respectively

ϕ porosity of the beach soil

ρ^* [ML^{-3}] & ρ_0^* [ML^{-3}] density of the beach pore water and the freshwater at 20 °C, respectively

ψ^* [L] & ψ dimensional and dimensionless pressure heads, respectively

References

Ataie-Ashtiani, B., Volker, R.E., Lockington, D.A., 1999a. Numerical and experimental study of seepage in unconfined aquifers with a periodic boundary condition. Journal of Hydrology (222), 165–184.

Ataie-Ashtiani, B., Volker, R.E., Lockington, D.A., 1999b. Tidal effects on sea water intrusion in unconfined aquifers. Journal of Hydrology 216 (1–2), 17–31.

Bokuniewicz, H., 1980. Groundwater seepage into Great South Bay, New York. Estuarine Coastal and Shelf Science 10, 437–444.

Boufadel, M.C., 2000. A mechanistic study of nonlinear solute transport in a groundwater–surface water system under steady state and transient hydraulic conditions. Water Resources Research 36, 2549–2565.

Boufadel, M.C., Suidan, M.T., Venosa, A.D., 1999a. A numerical model for density-and-viscosity-dependent flows in two-dimensional variably-saturated porous media. Journal of Contaminant Hydrology 37, 1–20.

Boufadel, M.C., Suidan, M.T., Venosa, A.D., 1999b. A numerical model for density-and-viscosity-dependent flows in two-dimensional variably-saturated porous media. Journal of Contaminant Hydrology 36, 1–20.

Boufadel, M.C., Suidan, M.T., Venosa, A.D., 1999c. Numerical modeling of water flow below dry salt lakes: effect of capillarity and viscosity. Journal of Hydrology 221, 55–74.

Boufadel, M.C., Suidan, M.T., Venosa, A.D., 1999d. Steady seepage in trenches and dams: effect of capillary flow. Journal of Hydraulic Engineering, ASCE 125, 286–294.

Cable, J.E., Burnett, W.C., Chanton, J.P., 1997. Magnitude and variations of groundwater seepage along a Florida marine shoreline. Biogeochemistry 38 (2), 189–205.

Cartwright, N., Jessen, O.Z., Nielseny, P., 2006. Application of a coupled ground–surface water flow model to simulate periodic groundwater flow influenced by a sloping boundary, capillarity and vertical flows. Environmental Modelling and Software 21, 770–778.

Cartwright, N., Nielsen, P., Liy, L., 2004. Experimental observations of watertable waves in an unconfined aquifer with a sloping boundary. Advances in Water Resources 27, 991–1004.

Colbert, S.L., 2004. Radium isotopes in San Pedro Bay, CA: constraint on inputs and use of nearshore distribution to compute nearshore dispersion rates. Ph.D. thesis, U. Southern California.

Croucher, A.E., O'Sullivan, M.J., 1995. The Henry problem for saltwater intrusion. Water Resource Research 31, 1809–1814.

Dracos, T., 1963. Ebene nichtstationare grundwasserabflüsse mit freier oberfläche., 57. Tech. Hochsch., Zurich, 114 pp.

Elder, J.W., 1967. Transient convection in a porous medium. Journal of Fluid Mechanics 27, 609–623.

Eslinger, D.L., Cooney, R.T., McRoy, C.P., Ward, A., Kline, T.C., Simpson, E.P., Wang, J., Allen, J.R., 2001. Plankton dynamics; observed and modelled responses to physical conditions in Prince William Sound, Alaska. Fisheries Oceanography 10 (1), 81–96.

Frind, E.O., 1982. Simulation of long-term transient density-dependent transport in groundwater. Advances in Water Resources 5, 73–88.

Galeati, G., Gambolati, G., Neuman, S.P., 1992. Coupled and partially coupled Eulerian–Lagrangian model of freshwater-seawater mixing. Water Resources Research 28 (1), 149–165.

Jeng, D.-S., Mao, X., Enot, P., Barry, D.A., Li, L., 2005. Spring-neap tide-induced beach water table fluctuations in a sloping coastal aquifer. Water Resources Research, 41.

Li, H.L., Jiao, J.J., 2003. Tide-induced seawater–groundwater circulation in a multi-layered coastal leaky aquifer system. Journal of Hydrology 274, 211–224.

Li, H.L., Li, L., Lockington, D., 2005. Aeration for plant root respiration in a tidal marsh. Water Resource Research, 41: W06023, doi:10.1029/2004WR003759.

Li, H.L., Zhao, Q.H., Boufadel, M.C., Venosa, A.D., 2007a. A universal nutrient application strategy for the bioremediation of oil polluted beaches. Submarine Pollution Bulletin 54, 1146–1161.

Li, H.L., Li, G., Cheng, J., Boufadely, M.C., 2007b. Tide-induced head fluctuations in a confined aquifer with sediment covering its outlet at the sea floor. Water Resources Research, 43: doi:10.1029/2005WR004724.

Li, H.L., Li, L., Lockington, D., Boufadel, M.C., Li, G.Y., 2007c. Modelling tidal signals enhanced by a submarine spring in a coastal confined aquifer extending under the sea. Advances in Water Resources 30, 1046–1052.

Li, L., Barry, D.A., Stagnitti, F., Parlange, J.-Y., Jeng, D.-S., 2000. Beach water table fluctuations due to spring-neap tides: moving boundary effects. Advances in Water Research 23, 817–824.

Mao, X., Prommer, H., Barry, D.A., Langevin, C.D., Panteleit, B., Li, L., 2006. Three-dimensional model for multi-component reactive transport with variable density groundwater flow. Environmental Modelling and Software 21, 615–628.

Naba, B., Boufadel, M.C., Weaver, J.W., 2002. The role of capillary forces in steady-state and transient seepage flows. Ground Water 40 (4), 407–415.

Neuman, S.P., 1973. Saturated–unsaturated seepage by finite elements. Journal of Hydraulics Division, ASCE, HY 12, 2233–2250.

Nielsen, P., 1990. Tidal dynamics of the water table in beaches. Water Resources Research 26, 2127–2134.

Pinder, G.F., Gray, W.G., 1977. Finite Element Simulation in Surface and Subsurface Hydrology. Academic Press, New York, NY, p. 294.

Portnoy, J.W., Nowicki, B.L., Roman, C.T., Urish, D.W., 1998. The discharge of nitrate-contaminated groundwater from developed shoreline to marsh-fringed estuary. Water Resources Research 34 (11), 3095–3104.

Prieto, C., Destouni, G., 2005. Quantifying hydrological and tidal influences on groundwater discharges into coastal waters. Water Resource Research, 41: doi:10.1029/2004WR003920.

Robinson, C., Gibbes B., Li, L., 2006. Driving mechanisms for groundwater flow and salt transport in a subterranean estuary. Geophysics Research Letters, 33: L03402, doi:10.1029/2005GL025247.

Robinson, C., Li, L., Barry, D., 2007. Effect of tidal forcing on a subterranean estuary. Advances in Water Resources. doi:10.1016/j.advwatres.2006.07.006.

Slomp, C., Van Capellen, P., 2004. Nutrient inputs to the coastal ocean through submarine groundwater discharge: controls and potential impact. Journal of Hydrology 295, 64–86.

Taniguchi, M., 2002. Tidal effects on submarine groundwater discharge into the ocean. Geophysics Research Letters, 29(12): 1561, doi:10.1029/2002GL014987.

Taniguchi, M., Ishitobi, T., Shimata, J., 2006. Dynamics of submarine groundwater discharge and fresh–seawater interface. Journal of Geophysics Research, 111: C01008, doi:10.1029/2005JC002924.

Teo, H.T., Jeng, D.S., Seymour, B.R., Barry, D.A., Li, L., 2003. A new analytical solution for water table fluctuations in coastal aquifers with sloping beaches. Advances in Water Resources 26, 1239–1247.

Turner, I., 1993. Water table outcropping on macro-tidal beaches: a simulation model. Marine Geology 115, 227–238.

Uchiyama, Y., Nadaoka, K., Rolke, P., Adachi, K., Yagi, H., 2000. Submarine groundwater discharge into the sea and associated nutrient transport in a sandy beach. Water Resource Research 36 (6), 1467–1479.

Valiela, I., 1990. Transport of groundwater-borne nutrients from watersheds and their effects on coastal waters. Biogeochemistry 10 (3), 177–197.

van Genuchten, M.T., 1980. A closed-form equation for predicting the hydraulic conductivity of unsaturated soils. Soil Science and Society of America Journal 44, 892–898.

Venosa, A.D., Suidan, M.T., Wrenn, B.A., Strohmeier, K.L., Haines, J., Eberhart, B.L., King, D., Holder, E., 1996. Bioremediation of an experimental oil spill on the shoreline of Delaware Bay. Environmental Science and Technology 30, 1764–1775.

Werner, A.D., Lockington, D.A., 2006. Tidal impacts on riparian salinities near estuaries. Journal of Hydrology 328, 511–522.

Wise, W.R., Clement, T.P., Molz, F.J., 1994. Variably saturated modeling of transient drainage: sensitivity to soil properties. Journal of Hydrology 161, 91–108.

Wrenn, B.A., Suidan, M.T., Strohmeier, K.L., Eberhart, B.L., Wilson, G.J., Venosa, A.D., 1997. Nutrient transport during oil-